



# Contact mechanism between dissimilar materials under plastic deformation

Denis Salikhyanov <sup>a,b,\*</sup>

<sup>a</sup> Institute of New Materials and Technologies, Ural Federal University, 620002 Ekaterinburg, Russian Federation

<sup>b</sup> Institute of Engineering Science, Ural Branch of The Russian Academy of Sciences, 620049 Ekaterinburg, Russian Federation

## ARTICLE INFO

### Article history:

Received 9 April 2019

Accepted 16 July 2019

Available online 2 September 2019

### Keywords:

Clad metal composites

Joint deformation

Cold roll bonding

Contact surface

Dissimilar materials bonding

Interlayer boundary

## ABSTRACT

The description of the new contact mechanism between dissimilar materials during joint plastic deformation is proposed in this paper. To analyze the process of joint deformation of composite material layers, a multi-stage analytical model was developed based on the study of the contact interaction between the surfaces of the materials to be bonded using the slip line method. When mathematical simulation of the process of joint deformation of dissimilar materials, the influence of the geometrical surface profile of a harder layer of a composite, as a more significant factor, was estimated. For the entire range of influence of the investigated geometrical surface profile of a harder material of a composite, the final forming and stress state parameters in its intermediate zone were determined. To verify the analytical model, computer simulation of the process of joint deformation of composite material layers by the finite element method in two-dimensional formulation was carried out. The comparison of both solutions has confirmed the adequacy of the results obtained in the mathematical simulation. The theoretical model can be used in the development of bonding mechanisms between dissimilar materials, in the development of manufacturing technologies of new clad composite materials, as well as in the analysis and improvement of the existing manufacturing technologies of clad composite materials.

© 2019 Académie des sciences. Published by Elsevier Masson SAS. All rights reserved.

## 1. Introduction

A current development scope in metallurgical industry aims at increasing the economic efficiency of the manufacturing of clad metal composites (CMC), as well as their operational and mechanical properties. Nowadays, CMC is becoming more common in various industries – transport, aviation, shipbuilding, aerospace, defense, energy, oil-production, oil-refining etc. – due to the possibility of combining various properties in one material. This allows saving expensive materials, improving the reliability of constructions and equipment. As an example, steel–aluminum [1–5], magnesium–aluminum [6–8], copper–aluminum [9–11] clad composites, as well as steel-based composites [12], are being actively developed and introduced into the manufacturing of vehicles. The use of parts made of composites in car construction allows one to reduce their weight, improve their performance characteristics, and reduce carbon emissions into the environment.

Among the well-known manufacturing technologies of CMC (explosion welding, roll bonding, joint pressing and drawing, casting, overlay welding, powder coating, etc.), the technologies based on roll bonding of dissimilar materials are the

\* Corresponding author at: Institute of New Materials and Technologies, Ural Federal University, 620002 Ekaterinburg, Russian Federation.

E-mail address: [d.r.salikhyanov@urfu.ru](mailto:d.r.salikhyanov@urfu.ru).

most promising and cost-effective ones due to high productivity of the process, opportunity of automation and organization of large-scale manufacturing, high reliability of process and relative simplicity of quality control. Compared with the widespread explosion welding, CMC produced by the method of roll bonding have higher accuracy, quality and stability properties, as well as a lower level of tensile residual stresses [13,14].

The main limiting factor in the development of CMC manufacturing technologies by the method of roll bonding is the problem of obtaining strong and uniform bonds between its layers, ensuring the stability properties of the composites. Due to the complexity of the ongoing physicochemical processes at the interlayer boundary between materials during their joint deformation, determination of the optimal preparation of initial materials and deformation parameters (i.e. temperature, strain and strain rate) is a time-consuming task for each composite being developed. As a result, development of a manufacturing technology for new clad metal composites is invariably associated with a large amount of experimental work.

Thus, research on cold roll bonding process is the current scientific direction. In the open literature, studies have been carried out to understand the effects of surface cleaning, rolling conditions such as rolling pressure, heating temperature, pre-rolling annealing treatment, post-rolling annealing treatment, stacking, reduction, velocity and friction at the interface on the bonding quality [15,16]. It was pointed out [15–18] that surface preparation, normally consisting of degreasing followed by scratch brush cleaning, is of substantial significance regarding bonding strength.

### 1.1. Effect of surface conditions on bonding strength

The investigations regarding the effect of the preparation method for the contact surfaces of materials to be bonded are mostly empirical. Quantitative evaluation of contact surfaces is made through arithmetical mean roughness  $R_a$ , ten-point mean roughness  $R_z$ , ridge height  $H$ , mean pitch of roughness on ridges  $S$ , ridge wavelength  $W$ , hardness and surface texture. Research results can be found in [3,15–22]. It is important to note that there is no clear opinion on the optimal values of the roughness parameters –  $R_a$  and others –, as well as on the optimal values of contact surface hardness.

The influence of surface roughness and initial thickness of the sheets on the bonding strength of steel–aluminum clad materials was studied using belt grinding (abrasive 120, 60 and 40 grit) and wire brushing ( $\emptyset$  0.2 mm,  $\emptyset$  0.3 mm, and  $\emptyset$  0.5 mm) in [3]. The highest tensile shear strength for clad materials was achieved for the surface treatment method by belt grinding (40 grit) with a surface roughness value  $R_a$  of 5.8  $\mu\text{m}$ .

The influence of macro- and micro-surface engineering was evaluated in [15]. The macro-engineered surfaces had two various types of surface texture (“grooves” and “diamonds”) and two values of surface roughness  $R_a$  (0.05 mm, 0.25 mm); the preparation method was machining. The micro-engineered surfaces had surface roughness  $R_a$  equal to 0.58  $\mu\text{m}$ , 0.13  $\mu\text{m}$  and 0.03  $\mu\text{m}$ ; the preparation method was polishing. The best bonding quality was observed for micro-engineered surfaces with roughness  $R_a$  less than 0.58  $\mu\text{m}$ , but no marked improvement is observed when surface roughness is reduced further to 0.13  $\mu\text{m}$  and 0.03  $\mu\text{m}$ . The worst result obtained for macro-engineered surfaces was with a roughness value of 0.25 mm.

Samples with four different values of roughness  $R_a$  were created in [16]: polished;  $R_a = 1 \mu\text{m}$ ; 3  $\mu\text{m}$ ; 5  $\mu\text{m}$ . The highest bond strength was achieved with surface roughness of 1  $\mu\text{m}$ , while higher values of  $R_a$  are degrading bond quality. The experiment with the polished samples results in poor bond strength.

The influence of four different preparation options with values of the surface roughness  $R_z$  of the contact surfaces of metals to be bonded equal to 0.09  $\mu\text{m}$ , 1.5  $\mu\text{m}$ , 4.4  $\mu\text{m}$ , 14  $\mu\text{m}$  was estimated in [17]. The results of the tests showed that the highest tensile strength of the bonding was observed for the sample with surface roughness  $R_z = 0.09 \mu\text{m}$ , and the lowest for the sample with  $R_z = 14 \mu\text{m}$ . Also, it was found that, the greater the aspect ratio  $H/W$  (where  $H$  is ridge height,  $W$  is ridge wavelength), the higher the bond strength.

Samples of stainless steel with two different surfaces ground by 1000 and 80 grit SiC papers were made with surface roughness values  $R_a$  of 0.43  $\mu\text{m}$  and 0.95  $\mu\text{m}$ , respectively [19]. Under the same bonding conditions, except for the surface finish, a higher shear strength of the bonding was obtained for the smoother surface ( $R_a$  of 0.43  $\mu\text{m}$ ).

It was noted that preparation by using wire brushes after degreasing and before rolling the package provides the highest bonding strength [21]. In [22], it was found that, in comparison with degreasing without further processing, grinding after degreasing allows one to achieve a higher bonding strength. In [18] it was suggested that the coarser surface finish of the materials to be bonded leads to a lower bonding strength due to the small contact area of the ridges.

The bond strength between aluminum strips produced by cold roll bonding at different surface roughness values were assessed and measured by the peeling test [23]. Increasing surface roughness of strips increases average bond strength. This is because of the increasing rolling force and pressure as well as work hardening by enhanced surface roughness. The highest average peel strength was obtained for a surface roughness value  $R_a$  of 4.2  $\mu\text{m}$ .

It should be noted that, in the case of the cold deformation of dissimilar materials (cold roll bonding), the hardness of the oxide layers also affects the bond strength of a composite [1,20,24,25]. In [20], three kinds of surface hardening states of the steel sheet were obtained by different mechanical surface preparation methods: by rotating flap disc and steel circumferential brushes with  $\emptyset$  0.3 mm wires and  $\emptyset$  0.1 mm wires. The results of the investigation show that, the smaller the hardness of the steel surface, the higher the bonding strength. Thus, the highest bond strength was observed for steel surfaces treated with a flap disc. In [24], it is noted that bonding strength deteriorates with increasing thickness of the oxide layer. It was also found that, for most metals, the ratio of the hardness of the oxide layer to the hardness of the base metal does not have a significant effect [25].

In [26–28], different brushing conditions were investigated with the aim to understand the influence of the surface treatment on the bond strength of steel–aluminum clad composites manufactured by cold roll bonding. The effect of the main brushing parameters – the rotation speed, the pressing force, and the movement speed – on surface roughness and structure development were determined. In [26], it was found that the pressure force during wire-brushing was the primary factor influencing the bonding strength, followed by the processing temperature and the rotational speed of the brush.

## 1.2. Existing bonding mechanisms

Bonding of dissimilar materials by joint deformation in the manufacturing of CMC is a long-studied topic. Several mechanisms explaining the formation of bonds between different materials – diffusion, dislocation, film et al. – have been proposed, as well as their experimental confirmation has been performed at a qualitative and a quantitative level. From the literature [1,10,11,20,29–31], one of the best known mechanism describing the process of formation of the bond between dissimilar metals is the “film” theory consisting of the following four stages:

- (1) fracture of the cover layer;
- (2) surface expansion increasing the area of virgin surface;
- (3) extrusion of virgin material through cracks of the cover layer;
- (4) establishment of contact and bonding between virgin materials.

There are several models for calculating the bonding of dissimilar materials: the models of Bay [31], of Wright et al. [32], of Vaidyanath et al. [33], of Zhang and Bay [34], of Madaah-Hosseini and Kokabi [35], of Govindaraj et al. [36], of Cooper and Allwood [37], of Khaledi et al. [38]. Among them, the most common is the model of N. Bay, which allows one to quantify the bond strength for specific materials. The description of Bay's model is given in [1,31]. In the calculation model, the surfaces to be bonded are represented as ideally flat, covered with thin oxide films and other contaminants. When calculating the bond strength, two factors are taken into account – the degree of surface exposure of the materials to be bonded and the pressure at the interlayer boundary. Herewith it is necessary to set the empirical characteristics of the material – the fraction of film layer and the threshold surface exposure, at which bond formation occurs. To obtain the last characteristic, it is necessary to carry out an experimental study of interlayer surfaces of a series of CMC rolled at different reduction rates and subjected to a peeling test with the use of a scanning electron microscope (SEM).

Thus, the existing and widely used models for characterizing bond formation in CMC layers under plastic deformation does not allow us to take into account the conditions of the contact surfaces noted in many papers as critically important.

Based on the foregoing, the aim of the present work is the investigation of contact interaction between dissimilar material surfaces during plastic deformation, taking into account the influence of surface roughness and strength properties of the surface layer, development of the contact mechanism between dissimilar materials based on the investigation of contact interaction, the experimental verification of the developed contact mechanisms, and also the determination of the criteria for oxide layer fracturing.

## 2. Proposed mechanism of bonding of dissimilar materials

The process of bonding of composite material layers during joint plastic deformation is considered as the process of embedding the surface ridges of the harder material of a composite into the surface of the softer one. The suggested simplification can be considered as valid, since it is known that the roughness dimension of a metal surface ranges from one to a few dozen microns [15–17,19–22], while the thickness of oxide films ranges from one to a few dozen nanometers [1,39]. For example, at room temperature, the thickness of the oxide film for Al is 2–4 nm, for Fe 5–10 nm, and for Cu 10–20 nm. Therefore, the metal surface consists of ridges and cavities of various sizes covered with a thin oxide film, as shown in [40]. The most significant surface profile is that of the harder component, since the softer material fills the cavities on the harder material surface to a certain limit, changing its original shape and stress state during the process of joint plastic deformation [41]. A geometrical description of the surface of the harder material can be obtained by statistical processing of its profilogram with the separation of a deterministic component [42].

The slip line method and the finite element method were chosen for solving the problem. In accordance with the slip line method, the deformable state is flat, i.e. the movement of the particles takes place in one plane. The deformable material is set as an ideally plastic ( $Y = 2k$ , where  $Y$  is flow stress,  $Y = 1/\sqrt{2} \cdot \sqrt{(\sigma_1 - \sigma_2)^2 + (\sigma_2 - \sigma_3)^2 + (\sigma_3 - \sigma_1)^2}$ ,  $\sigma_i$  are principal stresses,  $k$  is shear stress).

For the formulation of the problem of contact interaction between surfaces of materials to be bonded by the slip line method, the surface of the harder material is represented by a series of repeated ridges as shown in Fig. 1, with the ridge height  $H$ , the width of the ridge base  $W$ , the half-angle of the ridge vertex  $\gamma$ . In practice, the described surface of a harder material in the form of longitudinal continuous ridges (isotropic roughness) corresponds to what can be obtained by the method of dry grinding for preparing the steel's surface [43,44]. In order to simplify the mathematical model, the surface of the softer material is described as ideally flat. Since the softer material is a deformable body, then its flow curves, i.e. the shear flow stress  $k$  (in accordance with the flat statement of the problem,  $k = Y/2$ ), are given as the initial data.

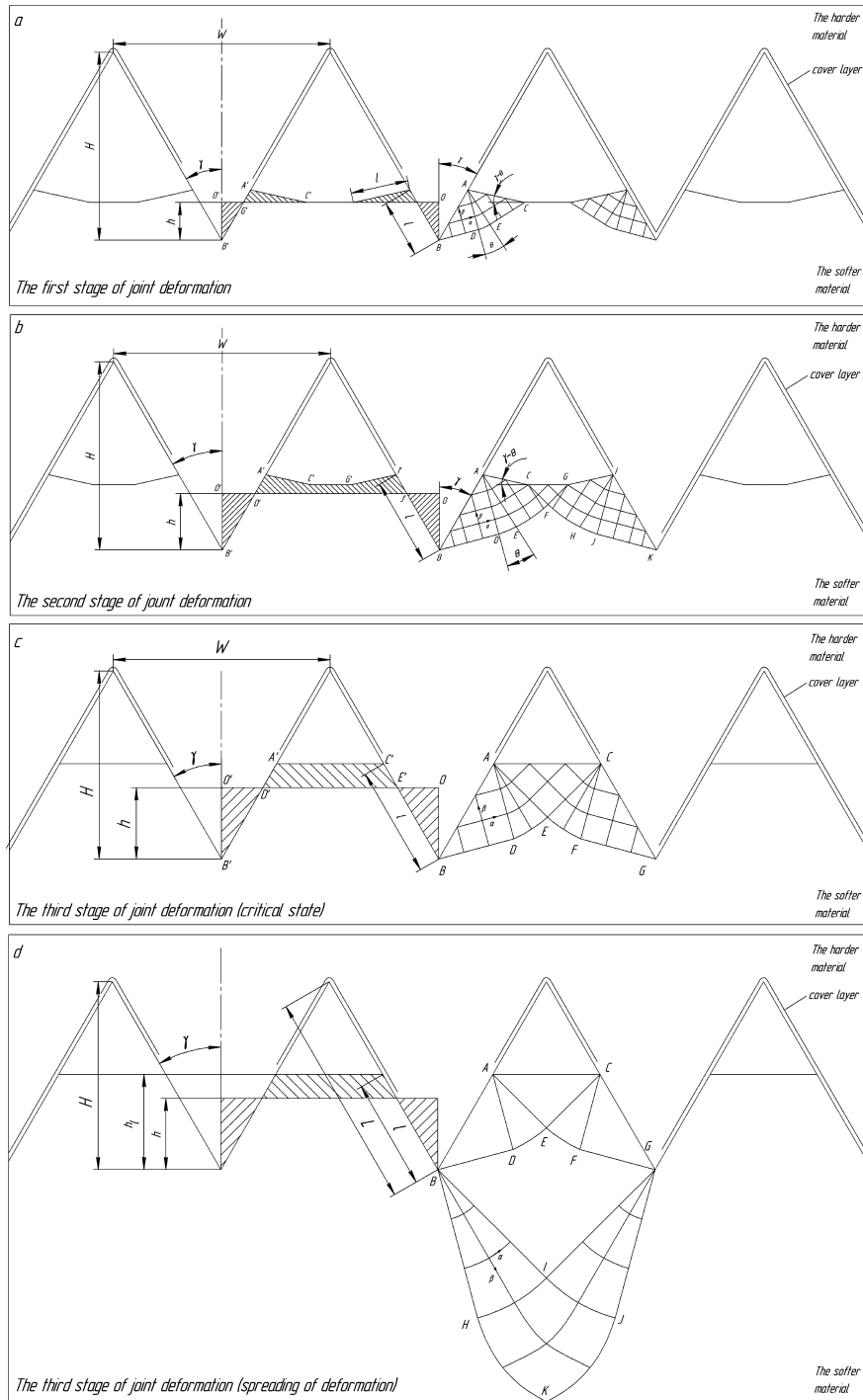


**Fig. 1.** Stages of the joint plastic deformation of dissimilar materials.

The process of bond formation between composite material layers during joint plastic deformation according to the proposed mechanism consists of the following stages (Fig. 1a–d).

- (1) Embedding of the ridges of the harder material into the softer one. The softer material is squeezed out from under the ridges into the cavities between them. Deformation zones from each ridge do not touch each other (Fig. 1a).

- (2) Filling the cavities of the harder material with the softer one, while deformation zones from each ridge in the softer material are in contact, forming the central deformation zone (Fig. 1b). Filling of the central zone occurs due to extrusion of the softer material from under both adjacent ridges.
- (3) The critical stage of filling the cavities of the harder material with the softer one – the flow of softer material into the cavities is difficult (Fig. 1c). Deformation begins to spread to the entire volume of the softer material (Fig. 1d).

For each stage of joint plastic deformation of dissimilar materials, the grid of slip lines was constructed and accordance with the kinematic conditions was checked: no gaps in the components of the metal particle displacement velocity normal to the lines separating the different areas of the grid of slip lines and fulfilment of the boundary conditions in velocities [45].

Depending on the ductile properties of oxide films on the surface of metals and the stress–strain state at the interlayer boundary, the fracturing of oxide films occurs, followed by extrusion of the virgin metal through cracks and establishment of bonding between virgin materials.

### 3. Study of the stress–strain state in the intermediate zone of the composite by the slip line method

Calculation of the stress–strain state parameters in the intermediate zone between dissimilar materials during joint plastic deformation was carried out in accordance with the slip line method. It was assumed that the softer material layer is stationary and that the harder material layer moves down with velocity  $v$ .

In the present work, the surface of the harder material is represented as a series of repeated ridges, the ridge height  $H$  was taken equal to 10  $\mu\text{m}$ , the harder material being assumed to be a rigid body. The surface of the softer material is assumed to be ideally flat, the shear flow stress of the softer material  $k$  is equal to 100 MPa. The half angle of the ridge vertex  $\gamma$  was chosen as the variable parameter. The required parameters are the actual contact length between dissimilar materials on one single ridge  $l$  depending on the embedding depth  $h$  of the ridges of the harder material into the softer one and the stresses at the interlayer boundary.

#### 3.1. Calculation of forming in the first stage of joint deformation

The scheme of forming of the softer material and the grid of slip lines in the intermediate zone for the first stage of the joint deformation are shown in Fig. 1a. The grid of slip lines and the equation for calculating forming completely coincide with the classical problem of indentation of a wedge into the plastic half-space, solved by R. Hill et al. [45]. Until the ridges have been embedded to a certain limit and the deformation zones from the adjacent ridges touched each other, the parameters of the stress–strain state can be calculated using well-known formulas [45].

The ABDEC area is the deformation zone, AB is the line of actual contact of the softer material with the ridge of the harder one, AC is the shifted surface, the lengths of sections AB and AC are equal as known from [45]. The ABDEC area consists of two triangular areas ABD and AEC, as well as centered area ADE with unknown angle  $\theta$ . The volume of the softer material extruded by the ridge  $A'G'C'$  is equal to the volume  $O'B'G'$ . In accordance with the slip line method, the slip lines converge with the contact surface AB and the free surface AC at an angle of  $45^\circ$ , the maximum shear stresses act along the slip lines. In the AEC area, on the free surface AC, the average normal stress  $\sigma$  ( $\sigma = \sigma_2 = (\sigma_1 + \sigma_3)/2$ ) is equal to  $\sigma_C = -k$ , the characteristic angle is  $\varphi_C = \pi/4 - \gamma + \theta$ . In ABD area, the characteristic angle  $\varphi_B = \pi/4 - \gamma$ , and the average normal stress from the Hencky's equation [45] along the slip line  $\alpha$  is  $\sigma_B = -k(1 + 2\theta)$ .

The displacement velocity  $v$  at the BDEC boundary is zero and, according to the Geiringer's equation [45], the variation of  $v$  along the straight line  $\beta$  is zero everywhere. Here, the displacement velocity  $u$  on each line  $\alpha$  is constant, and on the contact surface with the ridge AB is equal to  $\sqrt{2}\sin\theta$ . At any moment, all particles move along lines  $\alpha$  with the same velocity, and AC surface is shifted to a parallel position. Thus, the position of the shifted surface can be calculated geometrically at any moment during embedding the ridges.

According to [45], the unknown angle  $\theta$  can be calculated from the equation

$$AB \cdot \cos \gamma - AC \cdot \sin(\gamma - \theta) = OB$$

or

$$l \cdot [\cos \gamma - \sin(\gamma - \theta)] = h \tag{1}$$

The angle  $\theta$  was calculated for different values of  $\gamma$  in the range from 5 to  $85^\circ$  with a step of  $5^\circ$ . The results of the calculation are shown in Table 1. The values of  $0^\circ$  and  $90^\circ$  were not calculated, since they do not correspond to the initial geometric conditions.

To calculate the length of the actual contact with the ridges  $l$ , the equation was drawn up based on the equality of the triangular areas  $O'B'G'$  and  $A'G'C'$ .

$$h^2 \operatorname{tg} \gamma = (l \cos \gamma - h) \cdot [l \cos(\gamma - \theta) + (l \cos \gamma - h) \operatorname{tg} \gamma] \tag{2}$$

**Table 1**

The results of calculation of the stress–strain state parameters in the intermediate zone under joint plastic deformation of dissimilar materials.

Half-angle of the ridge vertex $\gamma$ ( $^\circ$ )	Ridge height $H$ ( $\mu\text{m}$ )	Width of the ridge base $W$ ( $\mu\text{m}$ )	$H/W$ ratio	Actual contact length between materials $l$ ( $\mu\text{m}$ )	Embedding depth of the ridges $h_l$ ( $\mu\text{m}$ )	Average normal stress on the contact surface $\sigma_{ AB}$ (MPa)	Relative average normal stress on the contact surface $\frac{\sigma}{k} _{AB}$
5	10.0	1.75	5.72	1.49	1.48	−117.5	−1.17
10	10.0	3.53	2.84	2.63	2.59	−134.9	−1.35
15	10.0	5.36	1.87	3.57	3.44	−152.4	−1.52
20	10.0	7.28	1.37	4.37	4.11	−169.8	−1.70
25	10.0	9.33	1.07	5.11	4.63	−187.3	−1.87
30	10.0	11.55	0.87	5.85	5.07	−204.7	−2.05
35	10.0	14.00	0.71	6.60	5.41	−222.2	−2.22
40	10.0	16.78	0.60	7.42	5.68	−239.6	−2.40
45	10.0	20.00	0.50	8.36	5.91	−257.1	−2.57
50	10.0	23.84	0.42	9.49	6.10	−274.5	−2.75
55	10.0	28.56	0.35	10.90	6.25	−292	−2.92
60	10.0	34.64	0.29	12.74	6.37	−309.4	−3.09
65	10.0	42.89	0.23	15.31	6.47	−326.9	−3.27
70	10.0	54.95	0.18	19.15	6.55	−344.4	−3.44
75	10.0	74.64	0.13	25.52	6.61	−361.8	−3.62
80	10.0	113.43	0.09	38.22	6.64	−379.3	−3.79
85	10.0	228.60	0.04	76.38	6.66	−396.7	−3.97

The length of the actual contact with the ridge  $l$  was calculated depending on the depth of embedding of the ridges  $h$ . The calculation results are shown in Table 1. For each value of the half-angle of ridge vertex  $\gamma$ , the depth of embedding of the ridges  $h$  at which the second stage (Fig. 1b) of joint deformation of dissimilar materials begins was calculated. The second stage begins at the moment when the shifted surfaces from two adjacent ridges come into contact with each other. The criterion for the second stage beginning is represented by the inequality

$$l \sin \gamma + l \cos(\gamma - \theta) \geq W/2 \quad (3)$$

The left part of inequality (3) is the projection of the length of AB and AC on the X axis, the right part of inequality (3) is the half-length between adjacent ridge vertices. As soon as the left part of inequality (3) becomes equal to the right part, the deformation zones from adjacent ridges start to interact and the second stage of joint deformation begins.

### 3.2. Calculation of forming in the second stage of joint deformation

The second stage of joint deformation is characterized by the presence of the common area CGF in the deformation zone from two adjacent ridges, as shown in Fig. 1b. Since forming of the softer material due to embedding of the ridges is symmetrical, the shifted common surface CG is assumed to be parallel to the X axis. The volume of material displaced by the ridges  $O'B'D'$  and  $J'OB$  is equal to the volume  $A'C'G'I'J'D'$ . As the ridges are embedded and  $h$  increases, the volume of the common area CGF in the deformation zone and the length of the shifted common surface CG increase.

The second stage continues until the entire central triangular area becomes common for two adjacent ridges, as shown in Fig. 1c. The criterion for the beginning of the third stage was determined graphically and was represented by the inequality

$$l \sin \gamma + l \cos(\gamma - \theta) - W/2 \leq W/2 - l \sin \gamma \quad (4)$$

Inequality (4) was obtained through geometric transformations from Fig. 1b. For brevity, intermediate geometric transformations have not been shown. The left part of inequality (4) represents the distance between points C and G, the right part of inequality (4) represents the distance between points A and I. As soon as the left part of inequality (4) becomes equal to the right part, the ridges have no inclined surfaces AC and GI. The central deformation zone will be represented only as being parallel to the X axis surface. Therefore, with the fulfillment of condition (4), the second stage of the joint deformation ends, and the third stage begins.

### 3.3. Calculation of forming in the third stage of joint deformation

The third stage of joint deformation is characterized by the presence of a common triangular area AEC from two adjacent ridges, as shown in Fig. 1c. The shifted surface AC has no inclined areas and is parallel to the X axis. The volume of material shifted by the ridges  $O'B'D'$  and  $E'OB$  is equal to the volume  $A'C'E'D'$ . A feature of the third stage of joint deformation is the change in the kinematic field of slip lines: the displacement velocity  $u$  along the slip lines  $\alpha$ , which before this stage went from point B to the free surface, is now limited by the contact surface with the adjacent ridge at point C. A gap occurs in the normal component of the displacement velocity of particles of the softer material and the boundary conditions on

velocities are not satisfied. Further flow of the softer material into the cavity is difficult, filling of the cavities of the harder material surface is terminated.

In Table 1, the final parameters for filling the cavities of the harder material with the softer one are presented: the depth of embedding of the ridges taking into account the shifted softer material  $h_1$  (see Fig. 1d), the actual length of the contact surface of the softer material with the ridges of the harder one  $l$ .

The actual grid of slip lines for third stage of joint deformation is shown in Fig. 1d. ABD, ADE, AEC, CEF and CFG blocks are fixed (non-deformable) and move down with the ridges of the harder material. The flow of material is concentrated in the depth of the deformable softer material. The deformation zone is represented by concentric BIH and GJI areas, as well as a rectangular HIJK area. As the ridges of the harder material move, the deformation spreads over the entire volume of the softer material, go over to the macro level. Further forming can be calculated by the known formulas of mechanics of solids (theory of plasticity) for a specific process of metal forming (joint rolling, for example).

### 3.4. Calculation of the stress state in the intermediate zone

In the presented contact mechanism between dissimilar materials, the third stage of joint deformation at which the filling of the cavities on the harder material surface ends is of the greatest interest. The stress state in the intermediate zone is of interest because, in conjunction with the strain state, it determines the fracture of the surface oxide films and, therefore, the bonding of dissimilar materials. To determine the stresses on the contact surface between dissimilar materials AB (Fig. 1c), the free surface AC was considered. The average normal stress  $\sigma$  ( $\sigma = \sigma_2 = (\sigma_1 + \sigma_3)/2$ ) on it is equal to  $\sigma|_{AC} = -k$ , the characteristic angle  $\varphi = \pi/4$ . Then, the average normal stress on the contact surface between materials from the Hencky's theorem [45]  $\sigma|_{AB} = -k(1 + 2\gamma)$ . According to the substitution formulas [45,46], the stress state on the contact surface can be described as follows:

$$\begin{cases} \sigma_{xx} = -k(1 + 2\gamma) - k \sin\left(\frac{\pi}{2} - 2\gamma\right) \\ \sigma_{yy} = -k(1 + 2\gamma) + k \sin\left(\frac{\pi}{2} - 2\gamma\right) \\ \sigma_{xy} = k \cos\left(\frac{\pi}{2} - 2\gamma\right) \end{cases} \quad (5)$$

The results of calculation of the stresses in the intermediate zone between dissimilar materials are given in Table 1.

## 4. Study of the stress–strain state in the intermediate zone of the composite by the finite element method

In order to verify the developed mathematical model of contact mechanism, computer simulation of the process of joint plastic deformation of dissimilar materials by the finite element method (FEM) in two-dimensional formulation was carried out using the Deform-2D program. For comparison, three problems with different half-angles of the ridge vertex of the harder material  $\gamma$  were set: 30°, 45°, and 60°. The same conditions as in analytical solution to joint deformation of dissimilar materials, described in Section 3, were assumed: the surface of the harder material is represented as a series of repeated ridges, the harder material is supposed to be rigid non-deformable body, the surface of the softer material is assumed to be ideally flat, the shear flow stress of the softer material  $k$  is equal to 100 MPa, the softer material is accepted as ideally plastic. The softer material layer is stationary, the harder material layer moves down with velocity  $v$ . The problem setting for computer simulation is shown in Fig. 2.

The total height of the softer layer is chosen approximately equal to the five heights of the wedges  $H$  of the harder material. Further simulation showed that, in the first two stages of joint deformation, the deformation is concentrated in the intermediate zone. At the end of the second stage, after filling the cavities on the surface of the harder material with the softer one, the deformation spreads to the entire thickness of the soft layer. After this the simulation ends.

The actual contact length  $l$  and the relative average normal stress  $\sigma/k$  between dissimilar materials at the end of stage I and stage II were chosen as the parameters to be studied by computer simulation. It is worth to note that, in contrast to the slip line method, the average normal stress  $\sigma$  obtained through the finite-element method will be distributed non-uniformly, which more fairly reflects the real processes of metal forming. Therefore, for comparison, the mean value of the average normal stress  $\sigma$  over the length of contact between materials obtained by the finite element method was taken.

The results of the comparison are presented in Table 2. In general, the nature of the material flow during joint deformation was investigated using the velocity vector field (Fig. 3) and the distribution of maximum shear stresses (Fig. 4). Maximum shear stresses act in red areas, as shown in Fig. 4.

## 5. Results and discussion

In order to verify the developed mathematical model of the contact mechanism between dissimilar materials consisting of three stages, qualitative and quantitative comparisons with the results of FEM-simulation were carried out. Comparing

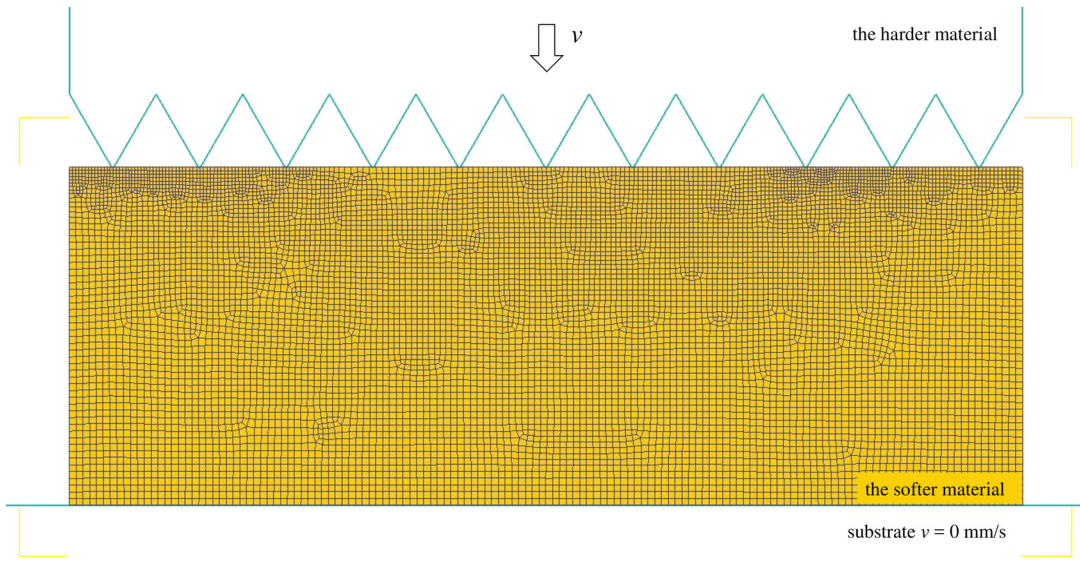


Fig. 2. Computer model for simulating joint deformation of dissimilar materials.

Table 2

Comparison of the actual contact length between materials and relative average normal stress at the interlayer boundary by mathematical and computer simulation.

Half-angle of the ridge vertex $\gamma$ (°)	30	45	60
The end of stage I and the beginning of stage II of joint deformation			
Length of the actual contact surface obtained from mathematical simulation $l_{\text{math}}^I$ ( $\mu\text{m}$ )	3.91	5.93	9.35
Length of the actual contact surface obtained from computer simulation $l_{\text{comp}}^I$ ( $\mu\text{m}$ )	3.93	6.24	8.88
Error amount $\Delta l/l$ (%)	0.51	5.23	5.29
End of stage II and beginning of stage III of joint deformation			
Length of the actual contact surface obtained from mathematical simulation $l_{\text{math}}^{II}$ ( $\mu\text{m}$ )	5.85	8.36	12.74
Length of the actual contact surface obtained from computer simulation $l_{\text{comp}}^{II}$ ( $\mu\text{m}$ )	5.61	8.26	12.18
Error amount $\Delta l/l$ (%)	4.28	1.21	4.6
Relative average normal stress on the contact surface obtained through mathematical simulation $\frac{\sigma}{k} _{AB}$	-2.05	-2.57	-3.09
Relative average normal stress on the contact surface obtained through computer simulation $\frac{\sigma}{k} _{AB}$	-2.11	-2.75	-3.24

the proposed stage-by-stage description of the process of joint plastic deformation of dissimilar materials (Fig. 1) and the computer simulation results (Fig. 3 and Fig. 4), qualitative coincidence of the sequence of stages can be seen.

For quantitative verification of the developed mathematical model, the actual contact length between materials  $l$  at the end of stages I and II of joint deformation and relative average normal stress  $\sigma/k$  at interlayer boundary were chosen. The results of comparison of pointed out parameters obtained by theoretical calculation and FEM-simulation are shown in Table 2. From Table 2 it is seen that error amount  $\delta_l$  calculated by the formula  $\delta_l = (l_{\text{comp}} - l_{\text{math}})/l_{\text{math}} \cdot 100\%$  does not exceed 5%, which indicates sufficient adequacy of the obtained results.

From both theoretical solution and computer simulation it follows that, in the whole range of roughness parameters ( $H/W$  or angle of ridge vertex  $2\gamma$ ), the filling of the cavities on the harder material surface will be incomplete in any case. After reaching the critical stage of filling of the cavities on the harder material surface with the softer material, the deformation will spread over the entire thickness of the softer material. This means that the actual contact length  $l$  (and actual contact area, if material width will be considered) between dissimilar material will not take the entire surface length  $L$  of the harder material ( $l$  and  $L$  are shown in Fig. 1d). The dependence of the relative actual contact length between materials  $l/L$  on the half-angle of ridge vertex  $\gamma$  at the end of the second stage of deformation is presented in Fig. 5a. The

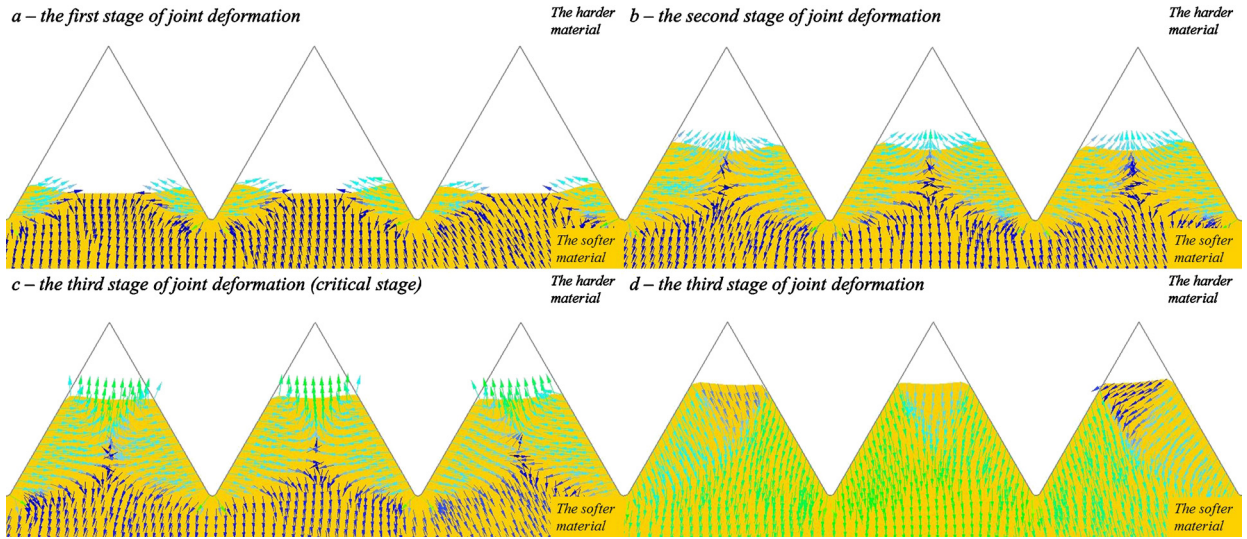


Fig. 3. Velocity vector field at different stages of joint plastic deformation of dissimilar materials observed by computer simulation.

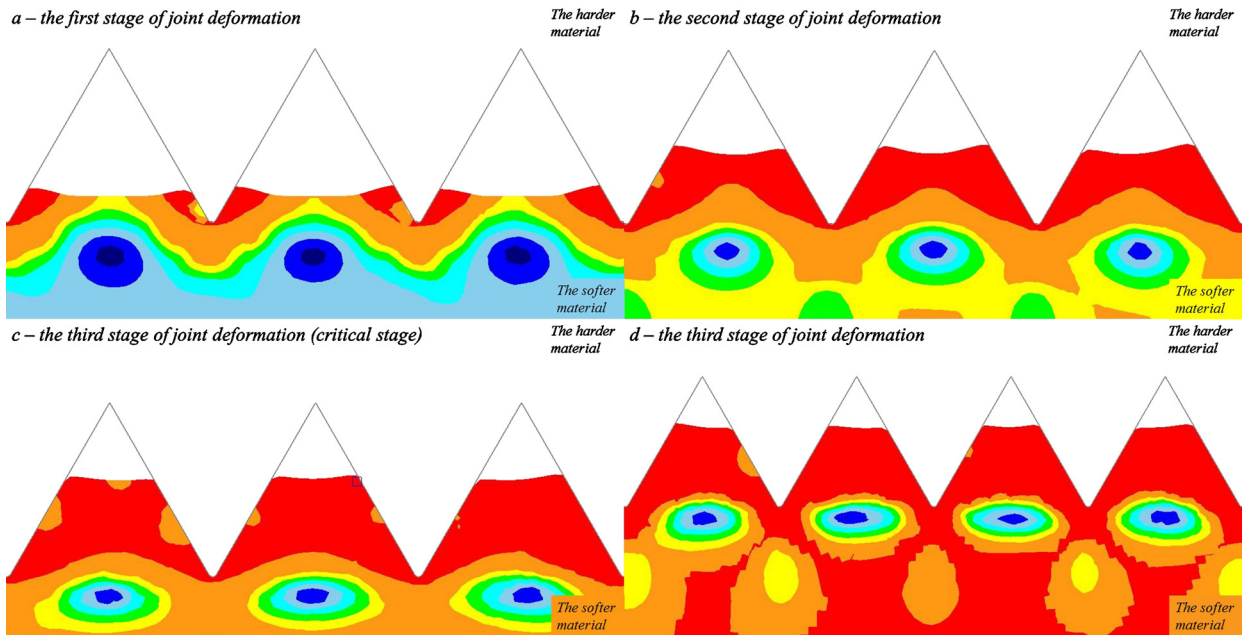


Fig. 4. Distribution of maximum shear stresses at different stages of joint plastic deformation of dissimilar materials observed by computer simulation (the red areas indicate the area of action of the maximum shear stresses).

dependence relation shows that, with an increase in the half-angle of ridge vertex  $\gamma$ , the relative actual contact length  $l/L$  also increases, the maximum value of the relative actual contact length  $l/L$  being 0.67.

This conclusion is confirmed by the experimental observations presented in [15,17]. In [17], Wang et al. investigate the effect of surface asperity on diffusion bonding of Cu with Cu through aspect ratio  $H/W$ , where  $H$  stands for ridge height,  $W$  for ridge wavelength. The surface of the samples consisted of longitudinal continuous ridges. The authors show the distribution of bonded areas on the fractured surface of the materials (Fig. 6). From the figures, it can be seen that almost all unbonded zones are long stria. It was suggested that voids formed on the bonding interface are pipes [17].

In [15], Liu et al. investigate the effect of macro- and micro-surface engineering on bond strength between dissimilar aluminum alloys during roll bonding. In their work, bonding between AA 2024 and AA 1100 aluminum alloys was studied. The flow stress of alloy AA 2024 is 270 MPa, while that of alloy AA 1100 is 40 MPa (according to the database of DEFORM-2D), so that these materials can be accepted as dissimilar, in accordance with the proposed contact mechanism. For the bonding of materials, one pass of rolling with reduction of 0.7% was applied. The authors prepared the surface of the harder material (AA 2024) in different ways. Two options correspond to the theoretical solution presented in this paper: longitudi-

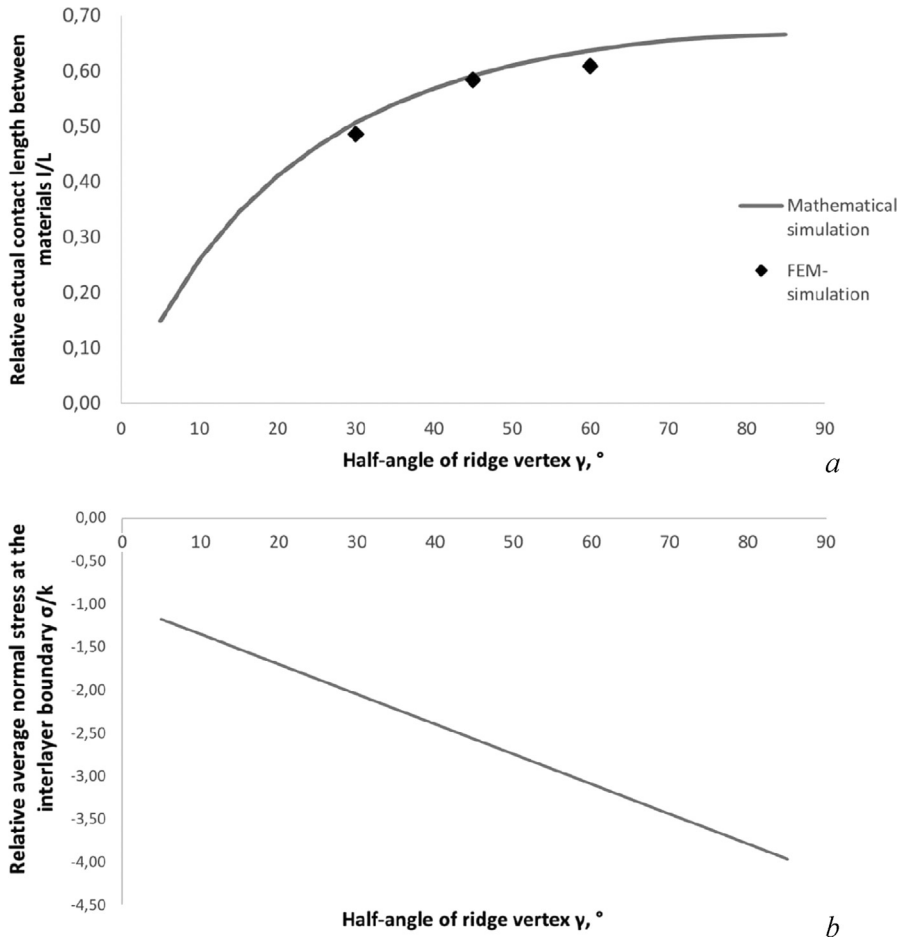


Fig. 5. (a) Dependence of relative actual contact length between materials on the half-angle of ridge vertex  $\gamma$ ; (b) dependence of the relative average normal stress  $\frac{\sigma}{k}$  on the half-angle of ridge vertex  $\gamma$ .

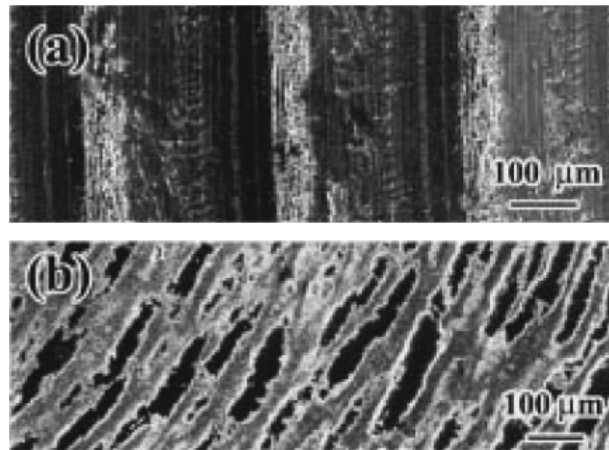
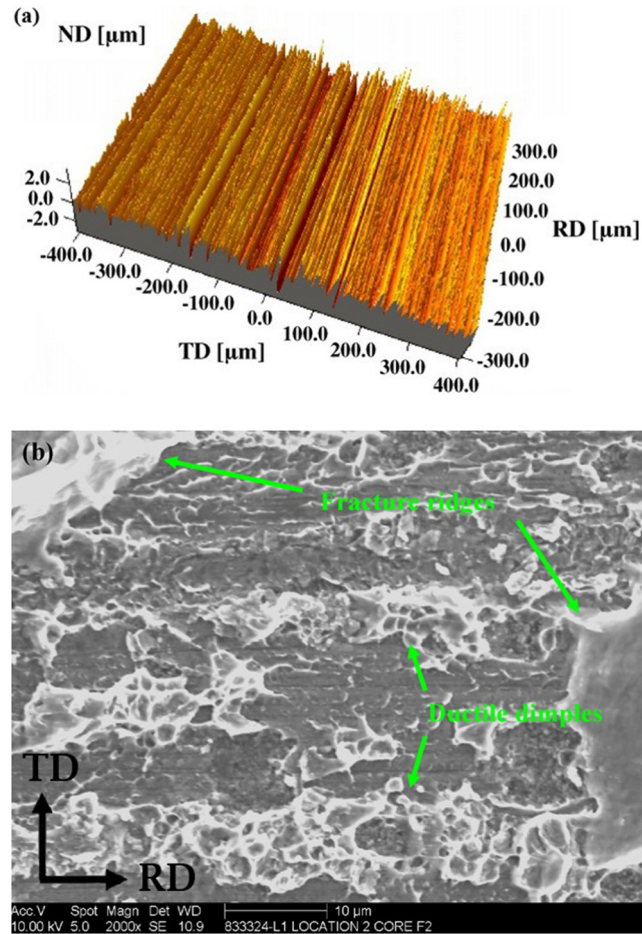


Fig. 6. Distribution of the bonded areas on contact surfaces [17]. (a) 14  $\mu\text{m}$ , 700  $^\circ\text{C}$ , 5.8 MPa, 20 min ( $H/W = 0.04$ ); (b) 90 nm, 400  $^\circ\text{C}$ , 5.8 MPa, 20 min ( $H/W = 0.004$ ). The bright zones are bonded areas, the dark zones are unbonded areas.

nal continuous ridges with the half-angle of ridge vertex  $\gamma$  equal to 60 $^\circ$  and the depth of the cavities of 0.05 and 0.25 mm. As a result of the joint deformation of these materials, delamination areas were found at the bonding interface for both options of the harder material surfaces. Based on microstructural studies, the authors suppose that the softer metal (AA 1100) failed to fully fill in the “valleys” on the harder material surface (AA 2024) and thus caused delamination. Moreover,



**Fig. 7.** (a) Surface of aluminum alloy AA 2024 with a roughness value  $R_a$  of  $0.58 \mu\text{m}$ ; RD is the rolling direction, TD is the transverse direction, ND is the normal direction; (b) SEM image showing the peeled surface of aluminum alloy AA 2024 with a roughness value  $R_a$  of  $0.58 \mu\text{m}$  [15].

the large intact surface area of the harder material with the deep texture (the depth of the cavities of  $0.25 \text{ mm}$ ) suggests that no bonding was ever established, which rules out the possibility of delamination of the initially bonded interface [15].

Also, some authors [15] have shown that the bonding interface was far from uniform by the example of bonding of alloys AA 1100 and AA 2024 by micro-surface engineering and with a roughness value  $R_a$  of  $0.58 \mu\text{m}$  (Fig. 7a). The unbonded areas (grey area) can be seen in Fig. 7b. Large amounts of fracture ridges and ductile dimples along the rolling direction found in bonded areas indicates substantial local deformation at the interlayer boundary during the peel test [15].

Thus, the unfilled cavities at the interlayer boundary between similar or dissimilar materials with rough surfaces can be observed as a result of joint plastic deformation, which corresponds to the conclusions made in this work concerning the theoretical solution.

Also, it is interesting to note that in [15] the authors pointed out the bonding strength between the hard and the soft material in bonded areas is even higher than the strength of the soft material. In accordance with the suggested contact mechanism, in the first two stages, deformation occurs near the interlayer boundary, and only after the critical stage, the deformation will spread further throughout the volume of the softer material. If we consider that in the case of cold deformation, real materials are hardenable, then it follows that the softer material in the intermediate zone will become harder than over the entire thickness. This may explain the noted effect.

In accordance with the foregoing, further filling of the cavities on the harder material surface is possible only after significant deformation, when the entire volume of the softer material becomes harder. This is consistent with the fact that increasing the deformation degree or rolling reduction improves the bond strength [11,21,23,35,36].

Regarding the contradictions on the optimal surface preparation and the roughness value noted in section 1.1., the following explanation can be given. As shown in section 1.1., part of the works [3,11,23] indicate that the coarser contact surface provides higher bond strength, part of the works [15,16,18,19] indicate the opposite, the smoother contact surface provides better bonding. Parks suggests in his work [18] that the coarser surface finish of the materials to be bonded leads to a lower bond strength due to the small contact area of the ridges. This assumption is in agreement with the proposed contact mechanism and graph in Fig. 5a. To establish a qualitative relation between roughness  $R_a$  and the half-angle of ridge

vertex  $\gamma$  shown in Fig. 5a, the relation between roughness  $R_a$  and slope angle  $\alpha$  can be accepted from [47]. The authors of [47] indicate that the higher roughness  $R_a$ , the higher the slope angle of the ridges  $\alpha$ . Accordingly, in our case, the higher roughness  $R_a$ , the lower the half-angle of ridge vertex  $\gamma$  and, consequently, the smaller the contact area.

A higher half-angle of ridge vertex  $\gamma$ , i.e. a smoother surface of the harder material, will provide a higher contact area, but it is necessary to pay attention to the relative average normal stress  $\sigma/k$  at the interlayer boundary between materials. The dependence of the relative average normal stress  $\sigma/k$  at the interlayer boundary on the half-angle of ridge vertex  $\gamma$  is presented in Fig. 5b. The dependence shows that the higher half-angle of ridge vertex  $\gamma$ , the higher compressive stresses must be applied to fill the cavities. At high angles of ridge vertex  $\gamma$ , a relative average normal stress  $\sigma/k$  2 to 4 times higher than the shear flow stress  $k$  of the softer material is observed. If the deformation degree and the applied normal stresses are small, then the filling of the cavities on the harder material surface and the actual contact area will be less.

This imposes a restriction on the properties of the harder material – its strength must be higher than the strength of the softer material. If this condition is not fulfilled, then plastic deformation of the harder material will begin too. Moreover, if the ductility of a harder material is low, joint deformation may cause cracks. It can be a possible explanation of the appearance of cracks on the steel surface at the interlayer boundary after joint plastic deformation of a steel–aluminum clad composite reported in [20].

Another reason for taking into account the relative average normal stress  $\sigma/k$  at the interlayer boundary is as follows. As mentioned earlier, the average normal stress  $\sigma = (\sigma_1 + \sigma_3)/2$ , where  $\sigma_1$  and  $\sigma_3$  are the principal stresses that act at the interlayer boundary. Respectively, the relative average normal stress  $\sigma/k$  indicates the fraction of tensile and compressive stresses: the higher  $\sigma/k$ , the greater the proportion of tensile stresses and vice versa. If  $\sigma/k$  is greater than 0, then tensile stresses prevail over compressive stresses; if  $\sigma/k$  is less than 0, then compressive stresses prevail over tensile stresses.

It is obvious that tensile stresses contribute to the fracturing of oxide films on metal surfaces; therefore, the greater the value of  $\sigma/k$ , the easier the fracture of oxide films on the metal surfaces. It can be seen from Fig. 5b that, at all angles of the ridge vertex  $\gamma$ , compressive stresses prevail over tensile stresses; besides, the larger the angle  $\gamma$ , the greater the proportion of compressive stresses. Hence, the rougher the harder material surface, i.e. the smaller the angle  $\gamma$ , the easier the fracture of oxide films on metal surfaces. This circumstance can explain why, in some research works, a coarser surface of the metals to be bonded contributes to higher bond strength.

In view of the above, it is suggested to calculate the fracturing of oxide films on the surface of metals to be bonded taking into account plasticity diagrams of oxide films. Then, the criterion for the fracturing of oxide films will take the form

$$\varepsilon \geq \varepsilon_f(\sigma/k)$$

where  $\varepsilon$  is the effective strain at interlayer boundary,  $\varepsilon_f$  is the critical effective strain at which the oxide film will fracture, and  $\varepsilon_f$  is the ductility of the oxide film, which is function of the relative average normal stress  $\sigma/k$ .

## 6. Conclusion

A description of the contact mechanism between dissimilar materials under plastic deformation taking into account the surface profile of the harder material of a composite was suggested; its theoretical analysis was carried out. The results of the theoretical calculation obtained by the slip line method and the results of computer simulation obtained by the finite element method show qualitative and quantitative coincidence. From the standpoint of theory of plasticity, the dependences of the depth of embedding of the ridges of the harder material into the softer one, the actual contact length between dissimilar materials, and the stress state at the interlayer boundary on the surface profile of the harder material were obtained.

The suggested mathematical model of contact mechanism between dissimilar materials under plastic deformation can be used for the development of the mechanism of bonding of dissimilar materials and can be useful for more accurate calculation of the bond strength between dissimilar materials. Besides, the theoretical model can be used for interpreting experimental results on the joint deformation of dissimilar materials.

The future directions of research work will take into account the influence of the three-dimensional surface profile of the harder material and the hardening of the materials to be bonded, and will investigate the bonding mechanism based on the proposed contact mechanism between dissimilar materials.

## Acknowledgements

The study was made within the basic part of the state job in the field of scientific activity No. 11.9538.2017/8.9 and was supported by Act 211 of the Government of the Russian Federation (agreement No. 02.A03.21.0006).

## References

- [1] R.-I. Mori, N. Bay, L. Fratini, et al., *CIRP Ann.* 62 (2013) 673–694.
- [2] S.V. Gladkovskii, T.A. Trunina, E.A. Kokovikhin, et al., *Met. Sci. Heat Treat.* 55 (1–2) (2013) 3–7.
- [3] M. Akdesir, D. Zhou, F. Foadian, H. Palkowski, *Int. J. Eng. Res. Sci.* 2-1 (2016) 169–177.
- [4] M. Movahedi, A.H. Kokabi, S.M. Seyed Reihani, *Mater. Des.* 32 (2011) 3143–3149.

- [5] M. Kleiner, M. Geiger, A. Klaus, *CIRP Ann.* 52 (2) (2003) 259–262.
- [6] J.-S. Lee, H.-T. Son, K.-Y. Lee, et al., *Adv. Mater. Res.* 26–28 (2007) 409–412.
- [7] M. Jafarian, M.S. Rizzi, M. Jafarian, *Mater. Sci. Eng. A* 666 (2016) 372–379.
- [8] M.J. Fernandes, T. Senthikumar, V. Balasubramanian, *Mater. Des.* 32 (2011) 1651–1656.
- [9] R. Uscinowicz, *Composites, Part B* 44 (2013) 344–356.
- [10] C.-Y. Chen, H.-L. Chen, W.-S. Hwang, *Mater. Trans.* 47 (4) (2006) 1232–1239.
- [11] K. Ozel, M. Sahin, A. Akdogan, *Stroj. Vestn., J. Mech. Eng.* 54 (11) (2008) 796–806.
- [12] T. Koseki, J. Inoue, S. Nambu, *Mater. Trans.* 55 (2) (2014) 227–237.
- [13] K.-I. Mori, *Adv. Mater. Res.* 966–967 (2014) 29–47.
- [14] L.M. Alves, C.M.A. Silva, P.A.F. Martins, *Key Eng. Mater.* 767 (2018) 25–41.
- [15] J. Liu, M. Li, S. Sheu, et al., *Mater. Sci. Eng. A* 479 (2008) 45–57.
- [16] A. Mikloweit, M. Bambach, M. Pietryga, G. Hirt, *Adv. Mater. Res.* 966–967 (2014) 481–488.
- [17] A. Wang, O. Ohashi, K. Ueno, *Mater. Trans.* 47 (2006) 179–184.
- [18] J.M. Parks, *Weld. J., Suppl.* 32 (1953) 209–222.
- [19] C. Zhang, H. Li, M. Li, *Vacuum* 137 (2017) 49–55.
- [20] C. Wang, Y. Jiang, J. Xie, *Mater. Sci. Eng. A* 652 (2016) 51–58.
- [21] H.D. Manesh, H.Sh. Shahabi, J. Alloys Compd. 476 (2009) 292–299.
- [22] M. Buchner, B. Buchner, B. Buchmayr, et al., *Int. J. Mater. Forming.* 1 (2008) 1279–1282.
- [23] R. Jamaati, M.R. Toroghinejad, *J. Mater. Eng. Perform.* 20 (2011) 191–197.
- [24] R.F. Tylecote, D. Howd, J.E. Furmidge, *Br. Weld. J.* 1 (1958) 21–38.
- [25] B.M. Agers, A.R. Singer, *Br. Weld. J.* 11 (1964) 313–319.
- [26] S. Reichelt, M. Schmidtchen, R. Kawalla, in: 14th International Conference on Metal Forming “METAL FORMING 2012” SPL, 2012, pp. 867–870.
- [27] S. Reichelt, H. Saleh, M. Schmidtchen, R. Kawalla, in: 8th International Conference on Processing and Manufacturing of Advanced Materials, THERMEC 2013, 783–786 (2014) 455–460.
- [28] M. Hosseini, M.H. Danesh, *Mater. Des.* 81 (2015) 122–132.
- [29] L. Da Silva, M. El-Sharif, C. Chisholm, S. Laidlaw, in: METAL 2014 - 23rd International Conference on Metallurgy and Materials, Conference Proceedings, 2014, pp. 274–284.
- [30] Khaledi, K., Rezaei, S., Wulfinghoff, S., Reese, S. (2019) Modeling of joining by plastic deformation using a bonding interface finite element, *Int. J. Solids Struct.*, 160, pp. 68–79.
- [31] N. Bay, *J. Eng. Ind.* 101 (1979) 121–127.
- [32] P.K. Wright, D.A. Snow, C.K. Tay, *Met. Technol.* 5 (1) (1978) 24–31.
- [33] L.R. Vaidyanath, M.G. Nicholas, D.R. Milner, *Br. Weld. J.* 6 (1959) 13–28.
- [34] W. Zhang, N. Bay, *CIRP Ann.* 45 (1996) 215–220.
- [35] H.R. Madaah-Hosseini, A.H. Kokabi, *Mater. Sci. Eng. A* 335 (1–2) (2002) 186–190.
- [36] N.V. Govindaraj, S. Lauvdal, B. Holmedal, *J. Mater. Process. Technol.* 213 (6) (2013) 955–960.
- [37] D.R. Cooper, J.M. Allwood, *J. Mater. Process. Technol.* 214 (2014) 2576–2592.
- [38] K. Khaledi, S. Rezaei, S. Wulfinghoff, S. Reese, *C. R. Mecanique* 346 (2018) 743–755.
- [39] A.G. Kobelev, et al., *Manufacturing of Clad Composite Materials, Internet Engineering, Moscow, 2002* (in Russian).
- [40] A. Almansour, M. Azizi, A.M. Jesri, S. Entakly, *Int. J. Acad. Sci. Res.* 3 (4) (2015) 37–45.
- [41] A.A. Bogatov, D.R. Salikhyanov, *Metallurgist* 60 (11–12) (2017) 1175–1179.
- [42] A.P. Husu, Yu.R. Vitenberg, V.A. Pal'mov, *Roughness of Surfaces (Statistical-Theoretic Approach)*, Nauka, 1975 (in Russian).
- [43] P.L. Menezes, Kishore, S.V. Kailas, in: *International Conference on Industrial Tribology, 2006*, pp. 1–15.
- [44] Yu.N. Loginov, *Izv. Vysš. Učebn. Zaved.* 5 (2004) 29–33.
- [45] R. Hill, *The Mathematical Theory of Plasticity*, Oxford University Press, 1998.
- [46] V.L. Kolmogorov, *Mechanics of Metal Forming, Metallurgy, Moscow, 1986* (in Russian).
- [47] G.W. Stachowiak, A.W. Batchelor, *Engineering Tribology*, 1993.